

**Manuscript version: Author's Accepted Manuscript**

The version presented in WRAP is the author's accepted manuscript and may differ from the published version or Version of Record.

**Persistent WRAP URL:**

<http://wrap.warwick.ac.uk/137163>

**How to cite:**

Please refer to published version for the most recent bibliographic citation information. If a published version is known of, the repository item page linked to above, will contain details on accessing it.

**Copyright and reuse:**

The Warwick Research Archive Portal (WRAP) makes this work by researchers of the University of Warwick available open access under the following conditions.

Copyright © and all moral rights to the version of the paper presented here belong to the individual author(s) and/or other copyright owners. To the extent reasonable and practicable the material made available in WRAP has been checked for eligibility before being made available.

Copies of full items can be used for personal research or study, educational, or not-for-profit purposes without prior permission or charge. Provided that the authors, title and full bibliographic details are credited, a hyperlink and/or URL is given for the original metadata page and the content is not changed in any way.

**Publisher's statement:**

Please refer to the repository item page, publisher's statement section, for further information.

For more information, please contact the WRAP Team at: [wrap@warwick.ac.uk](mailto:wrap@warwick.ac.uk).

# A Framework of L-HC and AM-MKF for Accurate Harmonic Supportive Control Schemes

Nishant Kumar, *Member IEEE*, Bhim Singh, *Fellow IEEE*, Jihong Wang, *Senior Member IEEE*, and Bijaya Ketan Panigrahi, *Senior Member IEEE*

**Abstract**— In this paper, an enhanced optimal control technique based on adaptive Maximize-M Kalman filter (AM-MKF) is used. To maximize power extraction from solar PV (Photovoltaic) panel, a learning-based hill climbing (L-HC) algorithm is implemented for a grid integrated solar PV system. For the testing, a three-phase system configuration based on 2-stage topology, and the deployed load on a common connection point (CCP) are considered. The L-HC MPPT algorithm is the modified version of HC (Hill Climbing) algorithm, where issues like, oscillation in steady-state condition and, slow response during dynamic change condition are mitigated. The AM-MKF is an advanced version of KF (Kalman Filter), where for optimal estimation in KF, an AM-M (Adaptive Maximize-M) concept is integrated. The key objective of the novel control strategy is to extract maximum power from the solar panel and to meet the demand of the load. After satisfying the load demand, the rest power is transferred to the grid. However, in the nighttime, the system is used for reactive power support, which mode of operation is known as a DSTATCOM (Distribution Static Compensator). The capability of developed control strategies, is proven through testing on a prototype. During experimentation, different adverse grid conditions, unbalanced load situation and variable solar insolation are considered. In these situations, the satisfactory performances of control techniques prove the effectiveness of the developed control strategy.

**Index Terms**—Solar PV Generation, Power Quality, Grid-Tied System, Adaptive Maximize-M Kalman Filter, DSTATCOM.

## I. INTRODUCTION

THE significant technological improvement has reduced the cost of the solar PV (Photovoltaic) array system [1]-[3]. Moreover, the static structure and pollution-free operation of SECS (Solar Energy Conversion System) show the suitability for small-scale to large-scale PV generation. Therefore, today SECS is highly popular [3]-[6]. However, the P-V (power-voltage) characteristic of a solar PV array is highly nonlinear, which shows the necessity of an advanced control technique. In general, the complexity of the control technique depends on topology and the number of assigned tasks. In this work, for power conversion, a topology of two-stage is considered, wherein its first stage, the maximum power is extracted from the panel [7], and in its 2<sup>nd</sup> stage, extracted DC solar power is changed in the form of AC, for feeding AC load and rest power is fed to the grid. In this task, the key objectives are MPPT (Maximum Power Point Tracking) for which a DC-DC converter is used, and the conversion from DC to AC, a voltage source converter (VSC) is used [8].

A literature survey on VSC control shows that several new algorithms are developed for reliable and robust operation. However, every control strategy has some merits and demerits, such as discrete Fourier transform-based control performs well in grid voltage distorted condition, but in a case of frequency variation, it suffers from an error during synchronization. Similarly, an adaptive notch filter [9] based control technique accurately estimates synchronizing frequency in the variable frequency situation, but its transient performance is poor. Kalman filter (KF) [10] based control technique gives a good performance during the transient condition, but its selection of convergence matrix is difficult. The weight least estimation technique [11] is free from algorithm parameter selection, but here high computational complexity is the main issue [12].

Some recently proposed techniques are space vector filter (SVF), multiple reference frames (MRF), moving average filter (MAF) [13], orthogonal component (OC), Butterworth bandpass filter (BBF) [14], least mean error based algorithm [15]-[17] etc. SVF control strategy performs very well in severe harmonics problem, and phase unbalance situation. However, similar to a discrete Fourier transform-based control, in a case of frequency variation, it suffers from an error during synchronization. BBF and MAF based control techniques perform very well in a steady-state condition. However, due to the high order of transfer function, its dynamic performance is poor. MRF and OC perform well in normal condition. However, during severe harmonics penetration in grid voltage, it is unable to generate accurate grid reference currents.

Therefore, in this paper, a novel AM-MKF (Adaptive Maximize-M KF) based control technique is developed for VSC control. This AM-MKF is an enhanced form of KF [18], where an AM-M (Adaptive Maximize-M) concept is used to enhance the estimation and filtering accuracy. The capability of developed AM-MKF control strategy is proven through testing on a prototype. During testing, different adverse grid conditions, unbalanced loads and variable solar insolation are considered. In these situations, satisfactory performances of control prove the motive of the developed control strategy.

The DC-DC converter is used for MPPT, which forces SECS to operate at MPP. A review of MPPT algorithms depicts that the most popular techniques are ‘perturb and observe’ (P&O) [19] and ‘incremental conductance’ (InC) [20]. The problems with these techniques are oscillations in a steady-state condition and deviation during dynamic change condition.

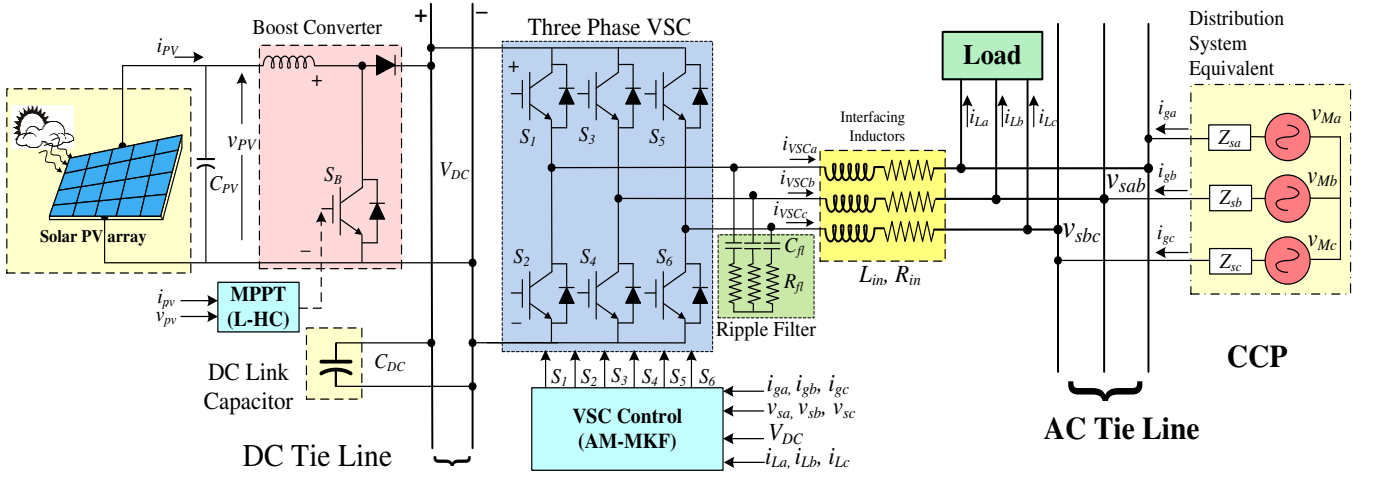


Fig.1 Three-Phase Two-Stage Grid-tied Solar PV system.

Some recently proposed techniques are, improved P&O [21] and modified InC [22], where the adaptive step-size concept is used. The issues with these techniques are, due to small step change, the oscillations in steady-state condition are less. However, in dynamics, it takes a longer time to reach the new MPP location. If a step change is increased, then algorithms performances are very good during the dynamics. However, large step-change creates oscillations in the steady-state condition. Therefore, these improvements are not upto the mark. For resolving all these above problems, in this work, the L-HC (Learning-based Hill Climbing) maximum power extraction algorithm is developed. The L-HC algorithm is the modified version of HC (Hill Climbing [23]) algorithm, where issues like, oscillations in steady-state condition and, slow response during dynamics are mitigated. The performance of the developed L-HC MPPT algorithm is proved through testing on a prototype. During experimentation, different types of solar irradiation changes are considered.

## II. SYSTEM CONFIGURATION

The configuration of three-phase two-stage grid-integrated SECS is illustrated in Fig.1. In this configuration, a boost converter is used for MPPT, which is controlled by L-HC MPPT algorithm. Using VSC, the generated PV power is converted into AC, where VSC is controlled by using AM-MKF based control. The output of VSC is connected on CCP (Common Connection Point) through interfacing inductor ( $L_{in}$ ,  $R_{in}$ ). On CCP, loads and grid are also connected. For removing switching ripples of VSC, a ripple filter is used ( $R_f$ ,  $C_f$ ) [24], which is also connected on CCP. The behavior of the system is based on the UPF (Unity power factor) operation. Moreover, in the nighttime, the system behavior is based on DSTATCOM operation. The used circuit parameters are given in Table-I.

## III. CONTROL APPROACH

The control scheme of grid integrated SECS is shown in Fig.2. Here, a complete control scheme is divided into 2 sections.

In the first section, the boost converter is operated for MPPT, which is controlled by L-HC algorithm. In this algorithm, the reference voltage ( $V_{ref}$ ) is estimated. By using  $V_{ref}$ ,  $\beta$  (duty cycle) is calculated for the boost converter, which forces SECS to operate at MPP.  $\beta$  is calculated as,

$$\beta = 1 - \frac{V_{ref}}{V_{DCref}} \quad (1)$$

Where  $V_{DCref}$  is DC-link reference voltage.

TABLE I  
CIRCUIT PARAMETERS

Parameter	Values	Parameter	Values
$V_{oc}$ at irradiance 1000W/m <sup>2</sup>	400V	$R_f$	10 $\Omega$
$I_{sc}$ at irradiance 1000W/m <sup>2</sup>	14A	$\nu$	5
$P_{load}$	1.24kW	$N_s$	20000
$v_a$	180V	$\epsilon$	40 $\times\omega_0$
$f$	50Hz	$d_{base}$	0.01
$L_{in}$	5mH	$\alpha$	1
$C_f$	10 $\mu$ F	$h$	1.1

The switching signal ( $S_B$ ) is generated through, comparing  $\beta$  with a saw-tooth wave. Adaptive  $V_{DCref}$  is calculated [24] as,

$$V_{DCref} = \sqrt{3} \times Y \times V_x \quad (2)$$

Where,  $V_x$  is grid voltage amplitude, and the component of loss compensation is  $Y$ .

At CCP, two-line grid voltages ( $v_{sab}$ ,  $v_{sbc}$ ) are sensed, and filtered using a decoupled bandpass filter. After this, the three-phase grid voltages ( $v_a$ ,  $v_b$ ,  $v_c$ ) are calculated as [25],

$$\begin{bmatrix} v_a \\ v_b \\ v_c \end{bmatrix} = \frac{1}{3} \begin{bmatrix} 2 & 1 \\ -1 & 1 \\ -1 & -2 \end{bmatrix} \begin{bmatrix} v_{sab} \\ v_{sbc} \end{bmatrix} \quad (3)$$

The  $V_x$  is derived as,

$$V_x = \sqrt{\frac{2}{3} (v_a^2 + v_b^2 + v_c^2)} \quad (4)$$

In-phase unit-templates ( $u_{pa}$ ,  $u_{pb}$ ,  $u_{pc}$ ) are calculated as,

$$u_{pa} = \frac{v_a}{V_x}, \quad u_{pb} = \frac{v_b}{V_x}, \quad u_{pc} = \frac{v_c}{V_x}, \quad (5)$$

For improving the dynamic performances of AM-MKF control algorithm, the impact of the instantaneous change in SECS on the grid currents, is considered by using a component of dynamic reflection of SECS ( $I_{Dpv}$ ) [24].  $I_{Dpv}$  is derived as,

$$I_{Dpv} = \frac{2 P_{pv}}{3 V_x} \quad (6)$$

For maintaining the required voltage on the DC link, the DC link voltage error is calculated and, it is minimized by PI (Proportional Integral) controller, which is derived as,

$$\left. \begin{aligned} e_{DC}(n) &= V_{DCref}(n) - V_{DC}(n) \\ \beta_{DC}(n+1) &= G_{P1} e_{dc}(n) + G_{I1} \int_0^n e_{dc}(n) dn \end{aligned} \right\} \quad (7)$$

Where,  $e_{DC}$  is the DC-link error, and the DC loss component is  $\beta_{DC}$ .  $G_{I1}$  and  $G_{P1}$  are PI controller integral and proportional gains, respectively.

Since loads are may be highly nonlinear, which consist of huge harmonic contents and shapes are close to quasi-square. Therefore, for deciding the active load power components ( $i_{loa}$ ,  $i_{lob}$ ,  $i_{loc}$ ), the load currents ( $i_{La}$ ,  $i_{Lb}$ ,  $i_{Lc}$ ) are filtered by AM-MKF, which extract in-phase fundamental components ( $k_a'$ ,  $k_b'$ ,  $k_c'$ ), quadrature components ( $k_a''$ ,  $k_b''$ ,  $k_c''$ ) and estimate fundamental frequency ( $C_f$ ).

$$\left. \begin{aligned} [k_a', k_a'', C_f] &= f_{AMUKF}(i_{La}) \\ [k_b', k_b'', C_f] &= f_{AMUKF}(i_{Lb}) \\ [k_c', k_c'', C_f] &= f_{AMUKF}(i_{Lc}) \end{aligned} \right\} \quad (8)$$

By using  $k_a'$ ,  $k_b'$ ,  $k_c'$  and  $k_a''$ ,  $k_b''$ ,  $k_c''$ , the amplitudes ( $A_a$ ,  $A_b$ ,  $A_c$ ) of FCs (fundamental components) are calculated as,

$$\left. \begin{aligned} A_a &= \sqrt{k_a'^2 + k_a''^2} \\ A_b &= \sqrt{k_b'^2 + k_b''^2} \\ A_c &= \sqrt{k_c'^2 + k_c''^2} \end{aligned} \right\} \quad (9)$$

$A_a$ ,  $A_b$ , and  $A_c$  are amplified by using  $C_f$ .

After it, the moving average filter (MAF) is used for estimation of active load power components ( $i_{loa}$ ,  $i_{lob}$ ,  $i_{loc}$ ). In MAF, the instantaneous value of the signal is calculated through the differences of integrated signal and  $N_s$ -step ( $N_s=f_s/C_f$ ) delayed of integrated signal, where the sampling frequency is  $f_s$ .

A component ( $\xi_p$ ) of active load current is derived as,

$$\xi_p = \frac{1}{3}(i_{loa} + i_{lob} + i_{loc}) \quad (10)$$

The equivalent component ( $\Phi_p$ ) of total loss is derived as,

$$\Phi_p = \beta_{DC} + \xi_p - I_{Dpv} \quad (11)$$

The grid current references ( $i_{ga}^*$ ,  $i_{gb}^*$ ,  $i_{gc}^*$ ) are generated as,

$$\left. \begin{aligned} i_{ga}^* &= u_{pa} \times \Phi_p \\ i_{gb}^* &= u_{pb} \times \Phi_p \\ i_{gc}^* &= u_{pc} \times \Phi_p \end{aligned} \right\} \quad (12)$$

By using hysteresis controller, the switching pulses of VSC ( $S_1$ ,  $S_2$ ,  $S_3$ ,  $S_4$ ,  $S_5$ , and  $S_6$ ) are produced, where the inputs are grid currents ( $i_{ga}$ ,  $i_{gb}$ ,  $i_{gc}$ ) and  $i_{ga}^*$ ,  $i_{gb}^*$ ,  $i_{gc}^*$ .

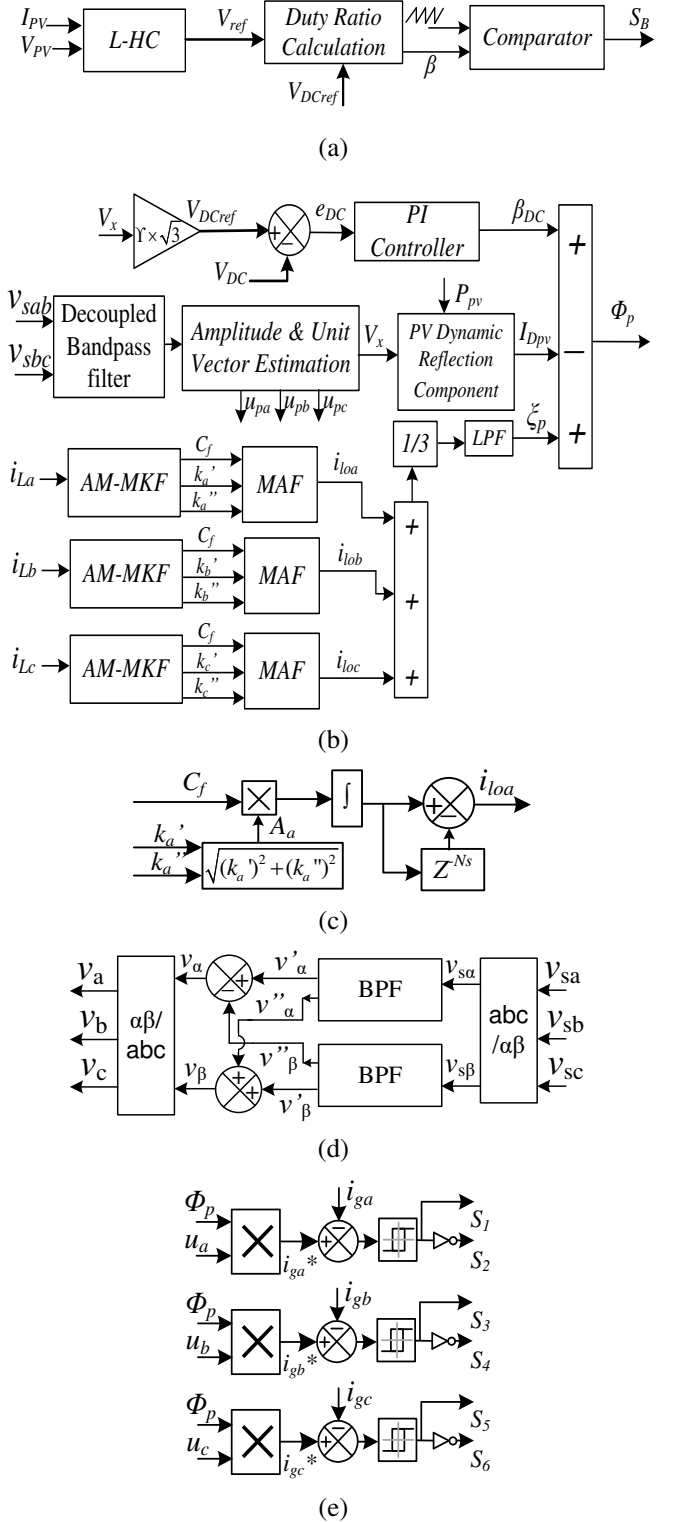


Fig.2 Control strategy for grid-tied SECS. (a) Control for boost converter, (b) VSC control, (c) MAF, (d) decoupled bandpass filter and (e) hysteresis control.

### A. Learning-based Hill Climbing (LHC) Algorithm

In learning-based hill climbing (LHC) algorithm, the existing issues of P&O [19] and InC [20] algorithms are resolved, such as oscillation issues in steady-state condition as well as, deviation and tracking duration related issues. In the literature, few modified techniques are available, which partially solves

these issues. In L-HC MPPT technique, all steady-state and dynamic conditions related issues are resolved.

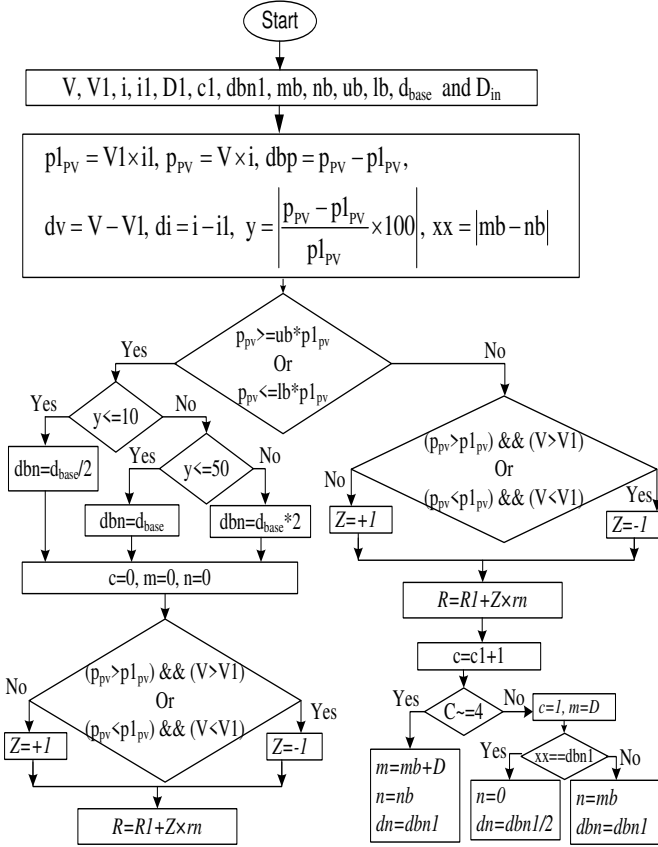


Fig.3 Flowchart of L-HC algorithm.

The flowchart of L-HC MPPT algorithm is shown in Fig. 3. The working strategy of L-HC algorithm is divided into two sections, the first section handles steady-state related issues, and the second section handles dynamics related issues.

In the first section, it detects the steady-state condition. After that, the step size is decreased according to the optimal duty cycle, which stops steady-state oscillation. In a second section, the dynamic condition is detected, and accordingly, the step size is increased. For condition detection, the envelop concept is used. In every iteration, the upper (*ub*) and lower (*lb*) layers are decided, which create power envelop. If generated solar power is in between the layers, then the condition is the steady-state condition. Otherwise, the situation is dynamic change condition. The *ub* and *lb* are derived as,

$$ub = \left( 100 + \left( \left( \frac{V_{oc}}{1 - d_{base}} \right) - V_{oc} \right) \times \frac{100}{V_{mpp}} \right) \times \frac{1}{100} \quad (13)$$

$$lb = \left( 100 - \left( \left( \frac{V_{oc}}{1 - d_{base}} \right) - V_{oc} \right) \times \frac{100}{V_{mpp}} \right) \times \frac{1}{100} \quad (14)$$

$$\left. \begin{aligned} (ub \times p1_{pv}) \geq p_{pv} \geq (lb \times p1_{pv}) &\Rightarrow \text{Steady State Condition} \\ \text{else} &\Rightarrow \text{Dynamic Condition} \end{aligned} \right\} \quad (15)$$

In a dynamic situation, the step change is derived as,

$$\left. \begin{aligned} \left| \frac{p_{pv} - p1_{pv}}{p1_{pv}} \times 100 \right| &\Rightarrow \begin{cases} \text{if } \leq 10, & \rightarrow dn = d_{base} / 2 \\ \text{if else } \leq 50 & \rightarrow dn = d_{base} \\ \text{else} & \rightarrow dn = 2 \times d_{base} \end{cases} \end{aligned} \right\} \quad (16)$$

In the condition of steady-state, the sum of three values of  $\beta$  is stored in '*nb*', and the next sum of three values of  $\beta$  is stored in '*mb*'. Using '*nb*' and '*mb*', a range of duty-cycle (*dbn*) is calculated as,

$$\left. \begin{aligned} \text{if } |mb - nb| = dbn1, &\Rightarrow n = 0, dbn = dbn1 / 2 \\ \text{else} &, \Rightarrow n = mb, dbn = dbn1 \end{aligned} \right\} \quad (17)$$

After it, the optimal value of *dbn*, is decided a new *D* (optimal duty cycle) is derived as follows,

$$\left. \begin{aligned} \text{if } p_{pv} > p1_{pv} \ \&\& \ V > V1 \\ \text{if } p_{pv} < p1_{pv} \ \&\& \ V < V1 \end{aligned} \right\} \Rightarrow Z = +1 \\ \text{Else} \Rightarrow Z = -1 \quad D = D1 - Z \times dbn \quad (18)$$

Where,  $p1_{pv}$ ,  $V1$ , and  $D1$  are previous power, voltage and duty cycle.

The performances of L-HC MPPT algorithm, in steady-state, as well as dynamic condition, are shown in experimental results (in the section- IV), which show oscillation free steady-state, and quick dynamic change performances.

### B. Adaptive Maximize-M Kalman Filter (AM-MKF)

The developed AM-MKF is a hybrid form of 'concept of adaptive maximize-M', 'Kalman filter [10]' and 'iterative particles update techniques', which objective is FC extraction from the load currents as well as from the grid voltages. In FC extraction process, AM-MKF filters the harmonic components and DC offset. In AM-MKF, Kalman filter estimates the FC from the signal. The estimation error is calculated by adaptive maximize-M technique, and it is minimized by 'iterative particles update techniques'. The mathematical process of AM-MKF is described as follows.

In the derivation, the state-space model is derived [18] as,

$$\left. \begin{aligned} k_a(i+1) &= g_i k_a(i) + Q_i \\ i_{La}(i) &= h_i^T k_a(i) + O_i \end{aligned} \right\} \quad (19)$$

Where,  $k_a$ ,  $i_{La}$ ,  $i$ ,  $Q_i$ ,  $g_i$ ,  $h_i$ , and  $O_i$  are state vector, input signal, sampling instant, process noise, state transition matrix, measurement matrix and measured noise, respectively.

The estimated  $Q_i$  is described as,

$$Q_i = k_a(i) - k_a(i-1) = D_i [y(i) - h_i k_a(i)] \quad (20)$$

Where,  $y(i)$  is input signal. Here, the load current is filtered by using AM-MKF, so  $y(i) = [i_{La}(i), i_{Lb}(i), i_{Lc}(i)]$ .

The working process of AM-MKF is described in as follows.

❖ State vector ( $\bar{k}_a(i+1)$ ) prediction

$$\bar{k}_a(i+1) = g_i k_a(i) \quad (21)$$

❖ Covariance matrix ( $\bar{C}_{i+1}$ ) prediction

$$\bar{C}_{i+1} = g_i C_i g_i^T + q_i \quad (22)$$

❖ Kalman gain matrix ( $D_i$ )

In AM-MKF,  $C_M(i)$  is generated using estimated and predicted data, where  $e_i(i)$  is the predefined value of maximum error.  $C_M(i)$  for  $C_M(i)$  matrix is calculated as,

$$C_M(i) = \begin{cases} 1 & \text{if } |k_a(i) - \bar{k}_a(i)| \hat{I} \max_{1 \leq l \leq J} (|e_l(i)|) \\ 0 & \text{Otherwise} \end{cases} \quad (23)$$

$C_M(i)$  is used in the derivation of conventional Kalman gain matrix, which enhances the accuracy in the estimation process. The modified Kalman gain matrix is derived as,

$$D_i = \frac{\bar{C}_i h_i^T \times C_M(i)}{C_M(i) \times h_i \bar{C}_i h_i^T + q'} \quad (24)$$

#### ❖ Estimation ( $k_a(i)$ ) update

In this process,  $C_M(i)$  is used to enhance the updating process, which reduces unnecessary damping in estimation process. The  $k_a(i)$  is derived as,

$$k_a(i) = C_M(i) \times \bar{k}_a(i) + D_i y(i) - D_i h_i \times C_M(i) \times \bar{k}_a(i) \quad (25)$$

#### ❖ Covariance matrix ( $C_i$ )

$$C_i = (I - D_i h_i) \bar{C}_i \quad (26)$$

Where,  $q_i$ ,  $T$ ,  $I$ , and  $q'$  indicate measurement noise, transpose matrix, identity matrix and process noise covariance matrix, respectively. the  $q_i$  is derived as,

$$q_i = \begin{bmatrix} [Q_1]^2 & 0 \\ 0 & [Q_2]^2 \end{bmatrix} \quad (27)$$

In this paper, AM-MKF is used for FC extraction from the load currents and grid voltages. Here, the derivation for phase-a, load current ( $i_{La}$ ) is given as follows.

The  $i_{La}$  is expressed as,

$$i_{La} = L_i(i) \sin(ij(i)R_s + W) \quad (28)$$

Where,  $R_s$  and  $i$  are sampling time and an integer harmonic component number. The instantaneous and initial phase angle are represented as  $\Omega$  and  $\Omega_0$ . From (28), the in-phase ( $k_a'$ ) component, and quadrature ( $k_a''$ ) component w.r.t. FC are derived, which are as,

$$\left. \begin{aligned} k_a'(i) &= L_i(i) \sin(j(i)R_s + W_0) \\ k_a''(i) &= L_i(i) \cos(j(i)R_s + W_0) \end{aligned} \right\} \quad (29)$$

Here,  $k_a(i) = [k_a'(i) \ k_a''(i)]^T$  is state vector. The predicted state vector is generated as,

$$\left. \begin{aligned} \bar{k}_a'(i+1) &= k_a'(i) \cos(j(i)R_s) + k_a''(i) \sin(j(i)R_s) \\ \bar{k}_a''(i+1) &= -k_a'(i) \sin(j(i)R_s) + k_a''(i) \cos(j(i)R_s) \end{aligned} \right\} \quad (30)$$

From (30),  $g_{iLa}$  is derived as,

$$g_{iLa} = \begin{bmatrix} \cos(j(i)R_s) & \sin(j(i)R_s) \\ -\sin(j(i)R_s) & \cos(j(i)R_s) \end{bmatrix} \quad (31)$$

Since, estimated and input voltage frequencies are equal, so  $h_{iLa} = [1 \ 0]$ . The block diagram for load currents is shown in Fig.4.

Similarly, the basic equations of AM-MKF for phase-b, and phase-c, the load currents are derived using (32)-(33).

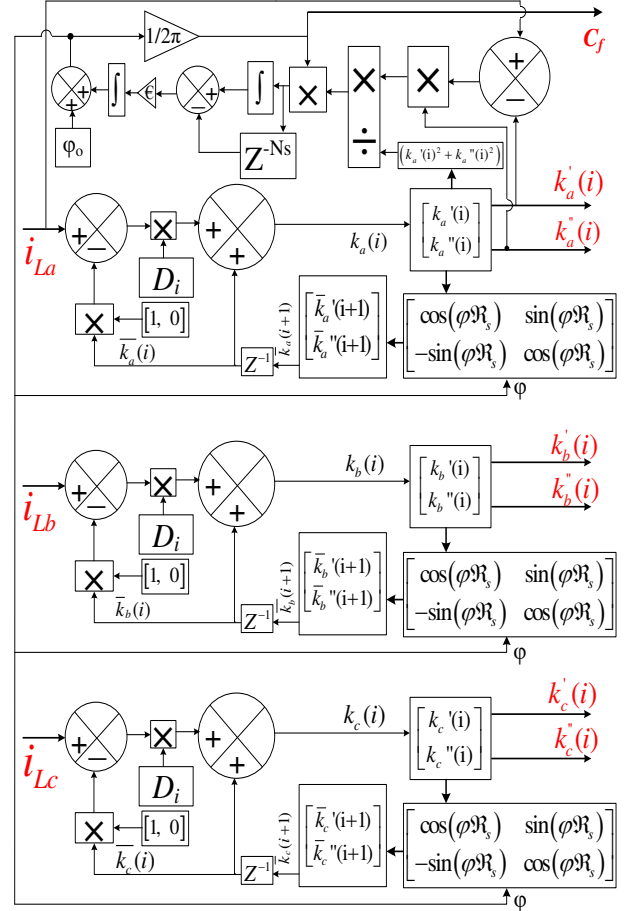


Fig.4 Block Diagram of AM-MKF.

$$\left. \begin{aligned} i_{Lb} &= L_i(i) \sin(i\varphi(i)R_s + \Omega) \\ k_b'(i) &= L_i(i) \sin(\varphi(i)R_s + \Omega_0) \\ k_b''(i) &= L_i(i) \cos(\varphi(i)R_s + \Omega_0) \\ \bar{k}_b'(i+1) &= k_b'(i) \cos(\varphi(i)R_s) + k_b''(i) \sin(\varphi(i)R_s) \\ \bar{k}_b''(i+1) &= -k_b'(i) \sin(\varphi(i)R_s) + k_b''(i) \cos(\varphi(i)R_s) \end{aligned} \right\} \quad (32)$$

$$\left. \begin{aligned} i_{Lc} &= L_i(i) \sin(i\varphi(i)R_s + \Omega) \\ k_c'(i) &= L_i(i) \sin(\varphi(i)R_s + \Omega_0) \\ k_c''(i) &= L_i(i) \cos(\varphi(i)R_s + \Omega_0) \\ \bar{k}_c'(i+1) &= k_c'(i) \cos(\varphi(i)R_s) + k_c''(i) \sin(\varphi(i)R_s) \\ \bar{k}_c''(i+1) &= -k_c'(i) \sin(\varphi(i)R_s) + k_c''(i) \cos(\varphi(i)R_s) \end{aligned} \right\} \quad (33)$$

### 1) Comparative Analysis of AMKF Algorithm

The comparative performance analysis of AM-MKF based control technique, with state of art techniques, such as SOGI [26], ANF [9] and KF [10] are illustrated in Fig. 5. The unbalanced load condition is considered, for comparative performance analysis, where phase-a load disconnection for 0.2s to 0.4s is taken. The waveforms of  $\xi_p$ , obtained by all techniques, are shown in Fig. 5. The waveform of ANF shows that during every dynamic change, huge oscillations are present in  $\xi_p$ . In the waveform of SOGI, the oscillations are very less, but the duration of reaching the steady-state condition is very large. In KF condition, overshoots are present in the obtained waveform. However, the obtained waveform by AM-MKF shows that oscillations are negligible, and overshoots are very less, as well as it quickly reaches the steady-state condition. It proves the objectives and shows the superiority over all state of art techniques. Moreover, since the value of  $\xi_p$  represents, information about the power requirement of the load, then the exact information about the load helps in accurate power conversion, which reduces the nonlinear current exchange with the grid. Therefore, power quality and the sinusoidal nature of the grid currents are properly maintained.

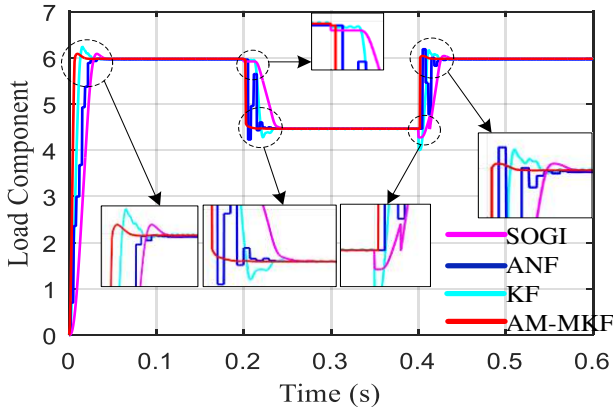


Fig.5 Responses of different algorithms.

## IV. RESULTS AND ANALYSIS

The developed L-HC MPPT and AM-MKF control techniques are tested on a prototype, which is shown in Fig.6. For the generation of P-V characteristic, a PV simulator is used, which is forced to operate at MPP by using a boost converter. For power conversion from AC-to-DC, a 2 level VSC is used, which output is attached on CCP through interfacing inductors. On CCP, the grid, as well as 3-phase load, is also attached. For mitigation of switching ripples of VSC, a RC filter is used on CCP. Hall-Effect current and voltage sensors are deployed for gathering electrical signals such as voltage and current.

### A. Operation under Normal Condition

The steady-state performance of phase-a, at solar irradiation  $1000 \text{ W/m}^2$ , where a nonlinear load is attached on CCP, is illustrated in Fig. 7.

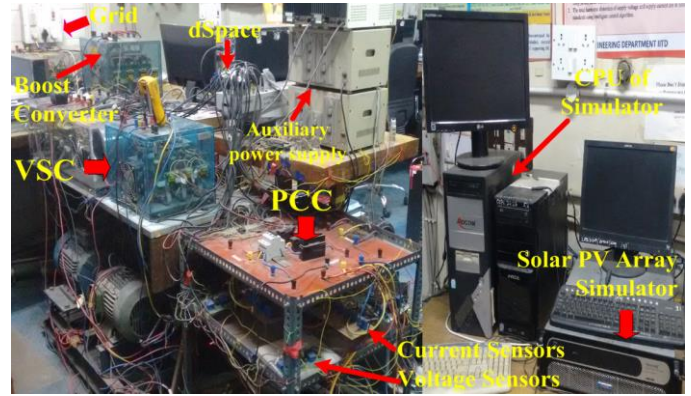


Fig.6 Photograph of the developed prototype.

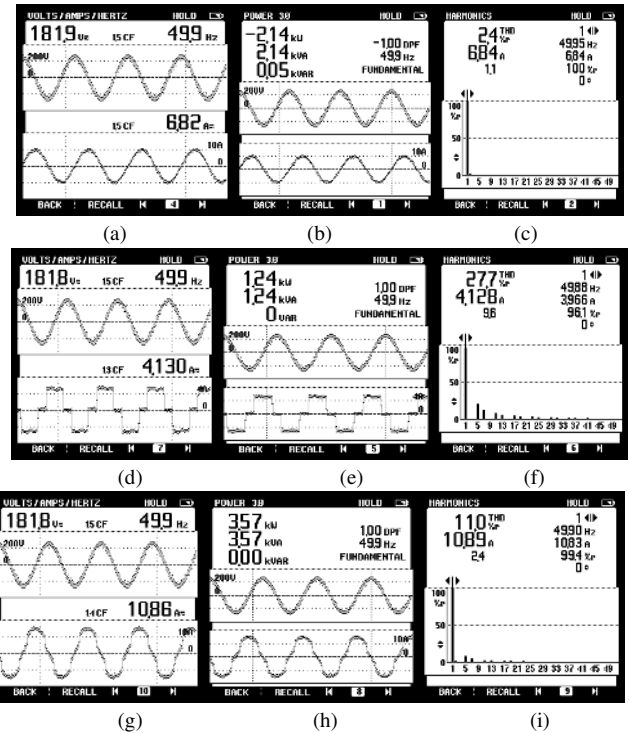


Fig.7 Waveforms at steady-state for phase 'a', (a)-(c) voltage, current, power and harmonic spectrum of grid current, (d)-(f) voltage, current, power and harmonic spectrum of load current, and (g)-(i) voltage, current, power and harmonic spectrum of VSC current.

Figs. 7(a)-(c) depict that the waveforms of  $v_a$  and  $i_{ga}$  show that the power is fed into the grid. During power feeding into the grid, the THD of  $i_{ga}$  is 2.4%, which is quite good. In Figs. 7(d)-(e), the waveform of  $i_{La}$  depicts that on CCP, nonlinear load is attached. The THD of  $i_{La}$  is 27.7%, as illustrated in Fig. 7(f). The harmonic currents of the load are provided by VSC, which are shown in Figs. 7(g)-(i). The waveform of  $i_{VSCa}$  is semi-sinusoidal, which shows that VSC generates harmonic currents according to the requirement of the load. The THD of  $i_{VSCa}$  is 11%, which is shown in Fig. 7(i).

### B. Operation under Load Unbalanced Condition

During testing at load unbalancing, the outage of phase-a load is considered, and obtained results are shown in Fig.8. In this operation, the obtained waveforms of phase-a and phase-b, are illustrated in Figs. 8(a)-(b). The internal signals of AM-MKF based control technique are illustrated in Fig.8(c). Fig. 8(a)

depicts that due to an outage of phase-a load, the  $i_{La}=0$ . Therefore, the requirement of harmonic currents is reduced, which improves the waveform of  $i_{VSCa}$ .

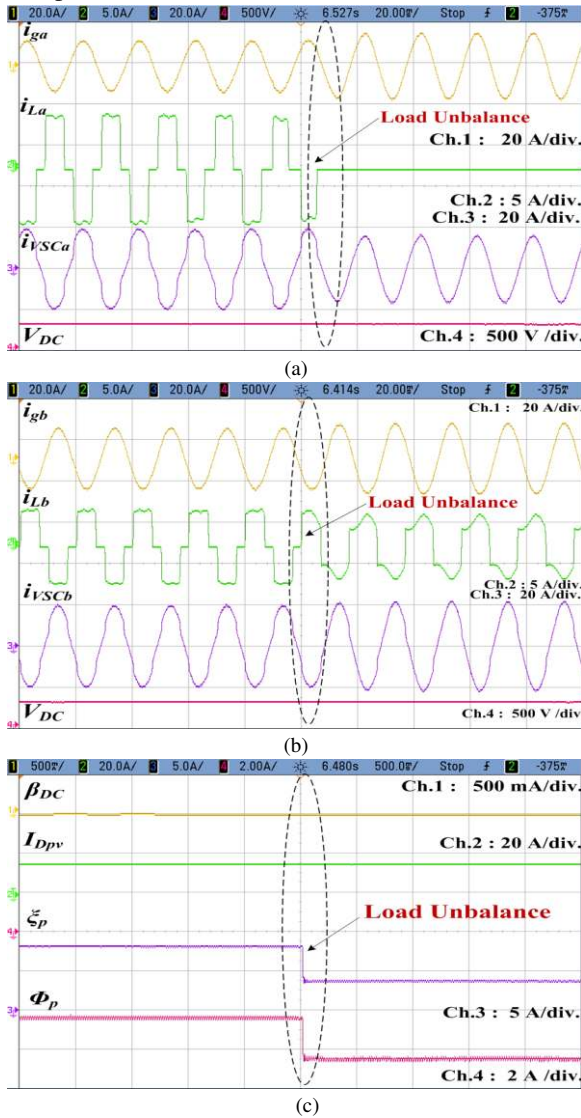


Fig.8 Waveforms during load unbalance, (a)-(b) grid current, load current, VSC current and DC link voltage of phase 'a' and 'b', (c) internal signals.

$V_{DC}$  is maintained constant because during the entire test, a constant solar irradiation  $1000\text{W/m}^2$  is considered. The waveform of  $i_{ga}$  depicts that it is slightly increased because due to the outage of phase-a load, the net requirement of load power is reduced. Moreover, due to the disconnection of phase-a load, the net nonlinearity of the load current is also decreased. Therefore, the waveform of  $i_{Lb}$  is improved, which is illustrated in Fig. 8(b). Fig.8(c) depicts that waveforms of  $\beta_{DC}$  and  $I_{Dpv}$  are maintained constant because the DC link voltage is balanced and no changes in the solar irradiation are considered. The  $\zeta_p$  is reduced because the requirement of load power is reduced. On -ve axis, the  $\Phi_p$  is also decreased, which indicates the increment of power flow towards the grid.

### C. Operation under Solar Irradiation Variation Condition

During testing at irradiance variation, the sudden irradiance fall, and rise, are considered. In irradiance fall condition, it is changed from  $1000\text{W/m}^2$  to  $800\text{W/m}^2$ . Similarly, during the irradiance rise condition, it is changed from  $800\text{W/m}^2$  to  $1000\text{W/m}^2$ . Here, for maximum power extraction, L-HC technique is used and its results are illustrated in Fig. 9. Fig.9 illustrates that during irradiance fall and rise, L-HC technique is taken  $0.28\text{s}$  and  $0.30\text{s}$ , respectively, which shows very good performance during the dynamic conditions. The waveforms show zero oscillation in a steady-state condition. Therefore, this technique illustrates the capability of oscillation related solution of conventional state of the art techniques.

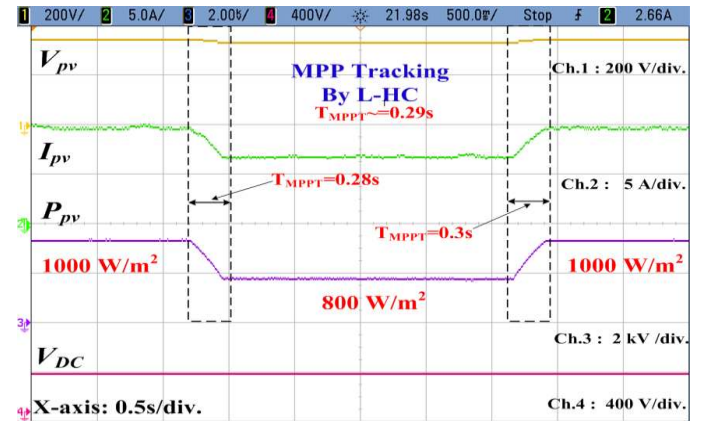


Fig.9 Waveforms during insolation fall.



Fig.10 Waveforms during the over-voltage condition.

### D. Operation during Grid Voltage Fluctuations Condition

Testing at grid voltage fluctuations on CCP, the overvoltage and under-voltage situations are considered. During an over-voltage, the voltage rise of 10% on CCP, is considered. Similarly, during the under-voltage, a voltage fall of 10% on CCP, is considered. In both conditions, the objective of the AM-MKF based control algorithm is to feed a sinusoidal current into the grid. Obtained results of phase-a, for over-voltage and under-voltage conditions, are shown in Figs.10-11, respectively. Moreover, for both conditions, the harmonic spectrum of  $i_{ga}$  is shown in Fig.12.



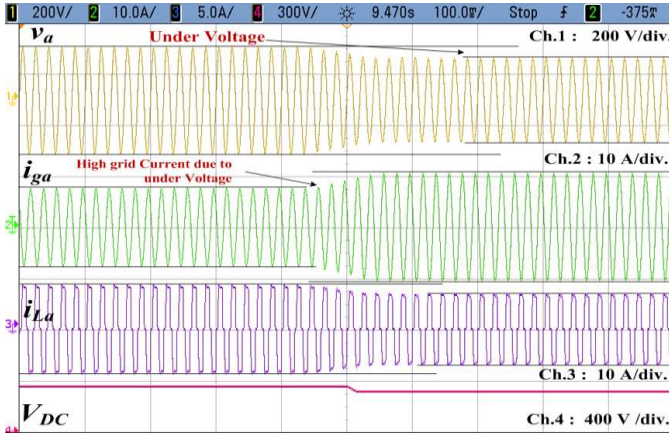
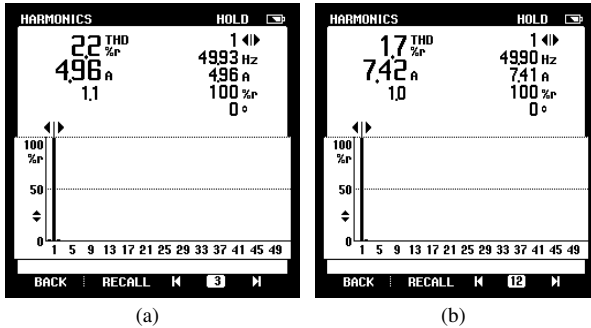


Fig.11 Waveforms during under-voltage condition.



(a)

(b)

Fig.12 Harmonic spectrum of  $i_{ga}$ , at (a) over-voltage and (b) under-voltage.

Fig. 10 reveals that due to overvoltage at CCP, the requirement of load power is increased. Therefore,  $i_{La}$  is increased. However,  $P_{PV}$  is constant, so the power is fed into the grid is decreased. Therefore,  $i_{ga}$  is decreased. Since, in this control, adaptive DC link voltage control is used. Therefore, DC link voltage is increased during an overvoltage. Similarly, Fig. 11 reveals that due to under-voltage at CCP, the requirement of load power is decreased. Therefore,  $i_{La}$  is decreased. However, the  $P_{PV}$  is constant, so the amount of power is fed into the grid is increased. Therefore,  $i_{ga}$  is increased. Since, in this control, adaptive DC link voltage control is used. Therefore, DC link voltage is decreased during under-voltage condition. Fig. 12 depicts that during, overvoltage, the THD of  $i_{ga}$  is 2.2%, and during under-voltage, the THD of  $i_{ga}$  is 1.7%. It indicates that in both situations, the AM-MKF based control technique is capable of feeding power with the pure sinusoidal current.

#### E. Operation during Grid Voltage Imbalance Condition

For the testing at unbalanced grid voltages on CCP, the three different voltages in three phases of the system are considered, and obtained waveforms are given in Figs.13-14.

In Fig.13, the waveforms of all three-phase grid voltages and grid currents are given. Moreover, in Fig.14, the vector diagram of all 3-phase voltages and currents are illustrated. Figs.13-14 depict that the voltages of three phases are 137.93V, 218.72V and 156.28V, which have 32.05% unbalance. However, in this situation, the obtained grid currents are 6.895A, 6.896A and 6.891A, which have only 0.01% unbalance. This performance proves that AM-MKF based

control technique is capable to feed balanced currents in highly unbalanced grid voltages conditions.

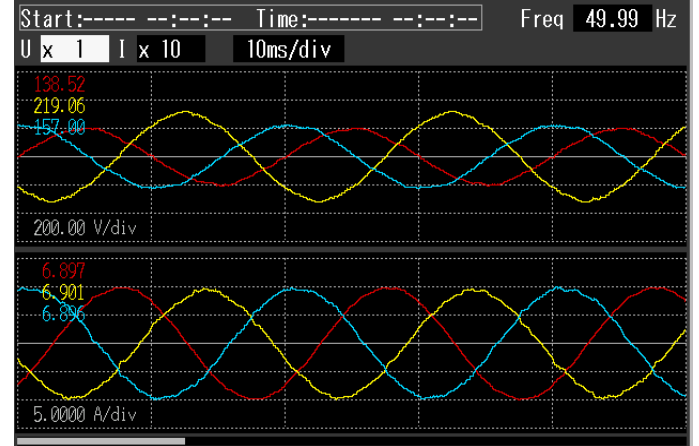


Fig.13 Waveforms of three-phase voltage and current during phase imbalance.

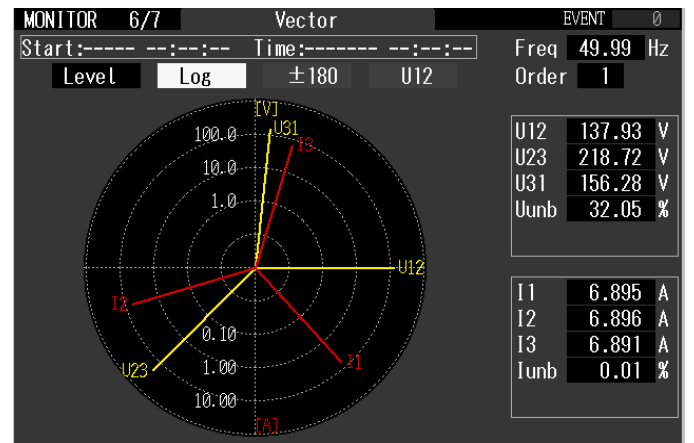


Fig.14 Vectors of three-phase voltage and current during phase imbalance.

#### F. Operation during Distorted Grid Voltage Condition

For the testing at distorted grid voltage condition on CCP, huge harmonic components in grid voltages are considered. In this situation, the objective of AM-MKF based control technique is to feed a sinusoidal current into the grid. The performances of AM-MKF based control technique, for phase-a, are illustrated in Fig.15. Moreover, the harmonic analyses of obtained output waveforms are given in Fig.16.

Fig.15 and Fig.16 depict that THDs of  $v_a$  and  $i_{La}$  are 6.4% and 27.7%. In this high harmonic distortion condition, the power is successfully fed into the grid. Therefore, the waveforms of  $v_a$  and  $i_{ga}$  are out of phase, which is illustrated in Fig.15 and Fig. 16(a). The waveforms of  $i_{La}$  and  $i_{VSCa}$  are also given in Fig.15, which depict that constant power is generated from SECS and a balanced power is fed to the load. Moreover, the waveform of  $i_{ga}$  is sinusoidal, which confirms the UPF operation. Fig. 16(b) depicts that the THD of  $i_{ga}$  is only 3.1%, which illustrates an efficient control ability in every adverse situation.

#### G. Operation during Day-to-Night Mode

During day-to-night or DSTATCOM mode of operation, two situations are considered. First, solar power is available, which is indicated as 'Day'. There, the PV panel generates power.

Second, solar power is not available, which is indicated as 'Night'. There, VSC generates reactive power. The combined performances of both situations are shown in Figs. 17-20.

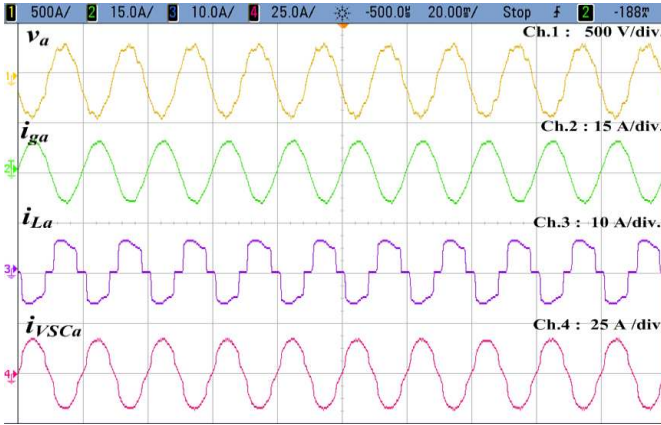


Fig.15 Waveforms under distorted grid voltage condition.

grid. The complete performances illustrate that in both the cases that the AM-MKF algorithm is capable to handle UPF operation and DSTATCOM operation.

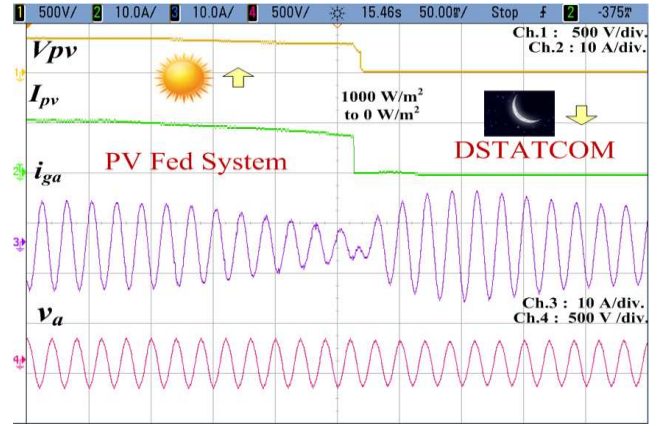


Fig.17 Waveforms of  $V_{pv}$ ,  $I_{pv}$ ,  $i_{ga}$  and  $v_a$ , during the day-to-night mode.

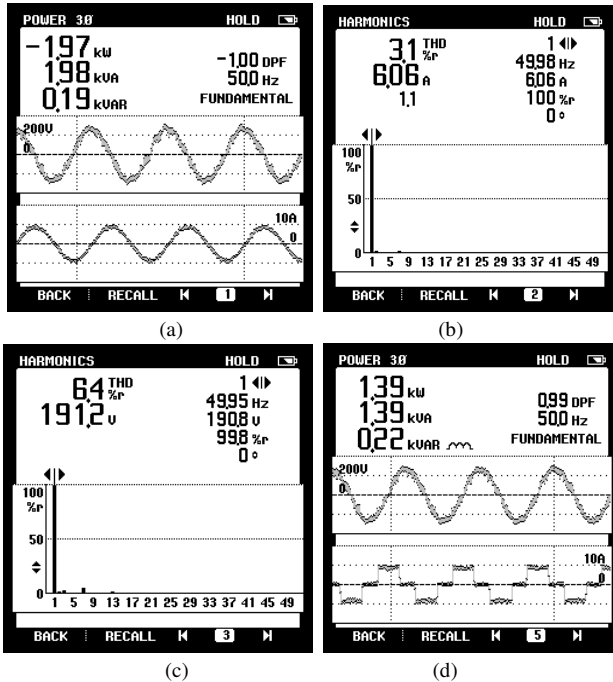


Fig.16 Waveforms of, (a)-(c) phase 'a' grid power and its harmonic spectra, and (d) phase 'a' load power, during distorted grid voltage condition.

Fig.17 and Fig.19 illustrate that during the daytime, the waveforms of  $i_{ga}$  and  $v_a$  are out of phase, which means power is fed into the grid. While in the nighttime, the waveform of  $i_{ga}$  and  $v_a$  are in the same phase, which means power is taken from the grid. The waveforms of  $V_{PV}$  and  $I_{PV}$  depict that in the daytime the power is produced, and in the nighttime, it is zero. Fig.18 and Fig.20 illustrate that in day and night, both times, a constant power is fed to the load. Moreover, constant  $V_{DC}$  is maintained during the entire operation. In the day time,  $V_{DCref}$  is calculated using an adaptive concept (2), and in the night time, according to CCP voltage, a fixed value is given.

The waveform of  $I_{VSCa}$  illustrates that in a daytime, VSC current is according to the available  $P_{PV}$ . However, in the nighttime, it is provided with reactive power support to the

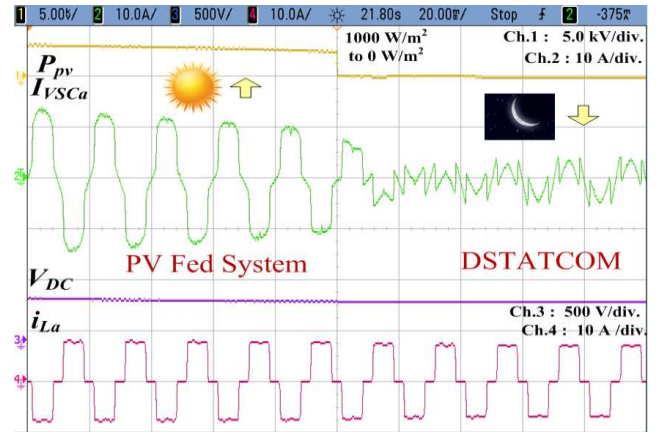


Fig.18 Waveforms of  $P_{pv}$ ,  $I_{VSCa}$ ,  $V_{DC}$  and  $i_{La}$ , during the day-to-night mode.

## V. CONCLUSION

A novel adaptive control technique namely, AM-MKF (Adaptive Maximise-M Kalman Filter) and a novel MPPT technique namely, L-HC (Learning-based Hill Climbing) have been developed for solar PV grid integrated system. The L-HC MPPT algorithm is a modified version of HC (Hill Climbing) algorithm, where issues like, oscillation in steady-state condition and, slow response during dynamic change condition are mitigated. The AM-MKF is an advanced version of KF (Kalman Filter), where for optimal estimation of accuracy of KF, an AM-M (Adaptive Maximize-M) concept is integrated. For testing, the three-phase system configuration based on 2-stage topology, where the deployed load on a common connection point (CCP) has been considered. The capability of developed control strategies has been proven through testing on the prototype. During experimentation, different adverse grid conditions, unbalanced load situation and variable solar insolation have been considered. In these situations, the satisfactory performances of the system have been proved the motive of the developed control strategy.

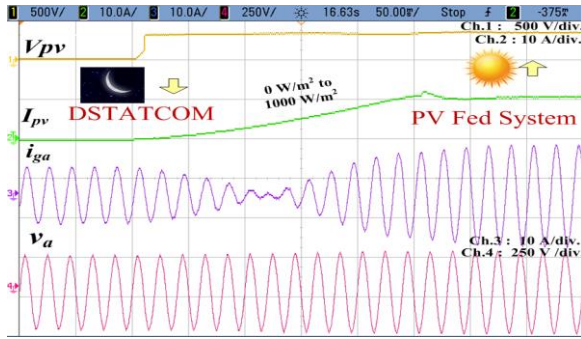


Fig.19 Waveforms of  $V_{pv}$ ,  $I_{pv}$ ,  $i_{gd}$  and  $v_{ad}$ , during the night-to-day mode.

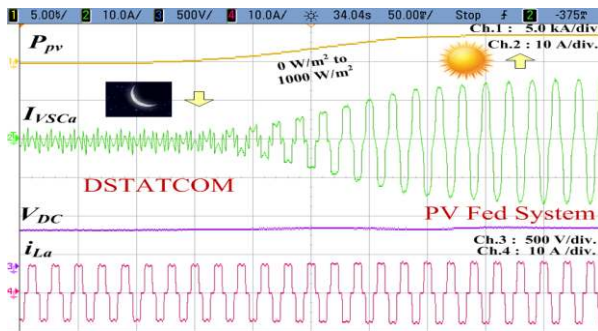


Fig.20 Waveforms of  $P_{pv}$ ,  $I_{VSCa}$ ,  $V_{DC}$  and  $i_{La}$ , during night-to-day mode.

#### REFERENCES

- [1] R. Wai and W. Wang, "Grid-Connected Photovoltaic Generation System," *IEEE Trans. Circuits and Systems I: Regular Papers*, vol. 55, no. 3, pp. 953-964, April 2008.
- [2] S. Biswas, L. Huang, V. Vaidya, K. Ravichandran, N. Mohan and S. V. Dhople, "Universal Current-Mode Control Schemes to Charge Li-Ion Batteries Under DC/PV Source," *IEEE Trans. Circuits and Systems I: Regular Papers*, vol. 63, no. 9, pp. 1531-1542, Sept. 2016.
- [3] J. Kim, J. Kim and C. Kim, "A Regulated Charge Pump With a Low-Power Integrated Optimum Power Point Tracking Algorithm for Indoor Solar Energy Harvesting," *IEEE Trans. Circuits and Systems II: Express Briefs*, vol. 58, no. 12, pp. 802-806, Dec. 2011.
- [4] M. Al-Soeidat, D. D. Lu and J. Zhu, "An Analog BJT-Tuned Maximum Power Point Tracking Technique for PV Systems," *IEEE Trans. Circuits and Systems II: Express Briefs*, vol. 66, no. 4, pp. 637-641, April 2019.
- [5] P. Zhang, G. Zhang and H. Du, "Circulating Current Suppression of Parallel Photovoltaic Grid-Connected Converters," *IEEE Trans. Circuits and Systems II: Express Briefs*, vol. 65, no. 9, pp. 1214-1218, Sept. 2018.
- [6] Y. Huang, D. Wang, L. Shang, G. Zhu, H. Tang and Y. Li, "Modeling and Stability Analysis of DC-Link Voltage Control in Multi-VSCs With Integrated to Weak Grid," *IEEE Trans. Energy Conversion*, vol. 32, no. 3, pp. 1127-1138, Sept. 2017.
- [7] A. B. Shitole, H. M. Suryawanshi, G. G. Talapur, S. Sathyan, M. S. Ballal, V. B. Borghate, M. R. Ramteke and M. A. Chaudhari, "Grid Interfaced Distributed Generation System With Modified Current Control Loop Using Adaptive Synchronization Technique," *IEEE Trans. Ind. Informatics*, vol. 13, no. 5, pp. 2634-2644, Oct. 2017.
- [8] Q. Hu, L. Fu, F. Ma and F. Ji, "Large Signal Synchronizing Instability of PLL-Based VSC Connected to Weak AC Grid," *IEEE Trans. Power Systems*, 2019. (Early Access)
- [9] S. Biricik, H. Komurcugil, N. Duc Tuyen and M. Basu, "Protection of Sensitive Loads using Sliding Mode Controlled Three-Phase DVR with Adaptive Notch Filter," *IEEE Trans. Industrial Electronics*, 2019 (Early Access).
- [10] S. Swain and B. Subudhi, "Grid Synchronization of a PV System with Power Quality Disturbances using Unscented Kalman Filtering," *IEEE Trans. Sustainable Energy*, 2019. (Early Access)
- [11] L. Shi and H. Zhao, "Diffusion Leaky Zero Attracting Least Mean Square Algorithm and Its Performance Analysis," *IEEE Access*, vol. 6, pp. 56911-56923, 2018.
- [12] Y. Sun, S. Li, B. Lin, X. Fu, M. Ramezani and I. Jaithwa, "Artificial Neural Network for Control and Grid Integration of Residential Solar Photovoltaic Systems," *IEEE Trans. Sustainable Energy*, vol. 8, no. 4, pp. 1484-1495, Oct. 2017.
- [13] S. Golestan, J. M. Guerrero and A. M. Abusorrah, "MAF-PLL With Phase-Lead Compensator," *IEEE Trans. Industrial Electronics*, vol. 62, no. 6, pp. 3691-3695, June 2015.
- [14] M. Ebrahimi, S. A. Khajehoddin and M. Karimi-Ghartemani, "Fast and Robust Single-Phase DQ Current Controller for Smart Inverter Applications," *IEEE Trans. Power Electronics*, vol. 31, no. 5, pp. 3968-3976, May 2016.
- [15] N. Kumar, B. Singh and B. K. Panigrahi, "LLMLF based Control Approach and LPO MPPT Technique for Improving Performance of a Multifunctional Three-Phase Two-Stage Grid Integrated PV System," *IEEE Trans. Sustainable Energy*, vol. 11, no. 1, pp. 371-380, Jan. 2020.
- [16] N. Kumar, B. Singh and B. K. Panigrahi, "PNKLMF-Based Neural Network Control and Learning-Based HC MPPT Technique for Multiobjective Grid Integrated Solar PV Based Distributed Generating System," *IEEE Tran. Ind. Infor.*, vol. 15, no. 6, pp. 3732-3742, June 2019.
- [17] N. Kumar, B. Singh and B. K. Panigrahi, "Framework of Gradient Descent Least Squares Regression-Based NN Structure for Power Quality Improvement in PV-Integrated Low-Voltage Weak Grid System," *IEEE Trans. Ind. Elect.*, vol.66, no.12, pp.9724-9733, Dec. 2019.
- [18] I. Kustiawan and K. Chi, "Handoff Decision Using a Kalman Filter and Fuzzy Logic in Heterogeneous Wireless Networks," *IEEE Communications Letters*, vol. 19, no. 12, pp. 2258-2261, Dec. 2015.
- [19] D. Sera, L. Mathe, T. Kerekes, S. V. Spataru and R. Teodorescu, "On the Perturb-and-Observe and Incremental Conductance MPPT Methods for PV Systems," *IEEE Journal of Photovoltaics*, vol. 3, no. 3, pp. 1070-1078, July 2013.
- [20] D. C. Huynh and M. W. Dunnigan, "Development and Comparison of an Improved Incremental Conductance Algorithm for Tracking the MPP of a Solar PV Panel," *IEEE Trans. Sustainable Energy*, vol. 7, no. 4, pp. 1421-1429, Oct. 2016.
- [21] M. Killi and S. Samanta, "Modified Perturb and Observe MPPT Algorithm for Drift Avoidance in Photovoltaic Systems," in *IEEE Trans. Industrial Elect.*, vol. 62, no. 9, pp. 5549-5559, Sept. 2015.
- [22] J. Ahmed and Z. Salam, "An Enhanced Adaptive P&O MPPT for Fast and Efficient Tracking Under Varying Environmental Conditions," *IEEE Trans. Sustainable Energy*, vol. 9, no. 3, pp. 1487-1496, July 2018.
- [23] H. Al-Atrash, I. Batarseh and K. Rustom, "Effect of Measurement Noise and Bias on Hill-Climbing MPPT Algorithms," *IEEE Trans. Aerospace & Elect. Systems*, vol. 46, no. 2, pp. 745-760, April 2010.
- [24] C. Jain and B. Singh, "A Three-Phase Grid Tied SPV System With Adaptive DC Link Voltage for CPI Voltage Variations," *IEEE Trans. Sustainable Energy*, vol. 7, no. 1, pp. 337-344, Jan. 2016.
- [25] Bhim Singh, Amrith Chandra and Kamal Al-Haddad, "Power Quality Problems and Mitigation Techniques," John Wiley & Sons Ltd, United Kingdom, 2015.
- [26] J. Matas, H. Martín, J. de la Hoz, A. Abusorrah, Y. A. Al-Turki and M. Al-Hindawi, "A Family of Gradient Descent Grid Frequency

Estimators for the SOGI Filter," *IEEE Trans. Power Electronics*, vol. 33, no. 7, pp. 5796-5810, July 2018.



**Nishant Kumar** (M'15) received the M.Tech. (with Gold Medal) degree in electrical power systems from the National Institute of Technology Durgapur, India, in 2013, and the Ph.D. degree (with Best Thesis Award) in power systems from the Department of Electrical Engineering, IIT Delhi, New Delhi, India, in 2019. He is currently working as a Postdoctoral Research Fellow at National University of Singapore (NUS) Singapore.

From 2013 to 2014, he was the Project Engineer/Research Associate at IIT Bombay and IIT Delhi. His areas of research interests include soft computing-based generation control, optimization algorithm development, and application of soft computing techniques in power system planning, operation, and control. Dr. Kumar has received the Gold Medal in M.Tech. degree from the National Institute of Technology Durgapur in 2013, Best Thesis award in PhD degree from IIT Delhi in 2019, 1st Prize in IEEE IAS Thesis Contest 2020 (PhD Category), and the POSOCO Power System National Award (PPSA-2018) in Doctoral Category from the Power Grid Corporation of India Limited in 2018.



**Bhim Singh** (SM'99, F'10) was born in Rahamapur, Bijnor (UP), India, in 1956. He has received his B.E. (Electrical) from the University of Roorkee (Now IIT Roorkee), India, in 1977 and his M.Tech. (Power Apparatus & Systems) and Ph.D. from the IIT Delhi, India, in 1979 and 1983, respectively. In 1983, he joined the Department of Electrical Engineering, University of Roorkee, as a Lecturer. He became a Reader there in 1988. In December 1990, he joined the Department of Electrical Engineering, IIT Delhi, India, as an Assistant Professor, where he has become an Associate Professor in 1994 and a Professor in 1997. He has been Head of the Department of Electrical Engineering at IIT Delhi from July 2014 to August 2016. He has been Dean, Academics at IIT Delhi, August 2016 to August 2019. He is JC Bose Fellow of DST, Government of India since December 2015. He is CEA Chair Professor since January 2019.

Prof. Singh has guided 83 Ph.D. dissertations, and 167 M.E./M.Tech./M.S.(R) theses. He has been filed 52 patents. He has executed more than eighty sponsored and consultancy projects. His areas of interest include solar PV grid interface systems, microgrids, power quality monitoring and mitigation, solar PV water pumping systems, improved power quality AC-DC converters..



**Jihong Wang** (M'06–SM'12) received the Ph.D. degree in nonlinear control theory from Coventry University, Coventry, U.K., in 1995.

She is currently a Professor of Electrical Power and Control Engineering with the School of Engineering, University of Warwick, Coventry, U.K. Her current research interests include nonlinear system control, system modeling and identification, power systems, energy efficient actuators and systems, and applications of intelligent algorithms. Dr. Wang was a Technical Editor for the IEEE TRANSACTIONS ON MECHATRONICS.



**Bijaya Ketan Panigrahi** (SM'06) received the Ph.D. degree in power system from Sambalpur University, Sambalpur, India, in 2004.

He was a Lecturer with the University College of Engineering, Sambalpur, for 13 years. Since 2005, he has been an Associate Professor in the Department of Electrical Engineering, Indian Institute of Technology (IIT) Delhi, New Delhi, India, where he has become a Professor in 2017.

His research interests include intelligent control of flexible ac transmission system devices, digital signal processing, power quality assessment, and application of soft computing techniques to power system planning, operation and control.